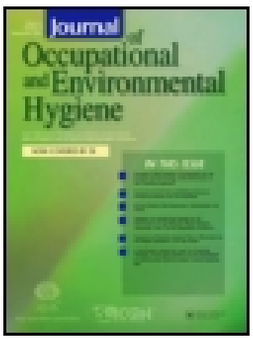

Journal of Occupational and Environmental Hygiene

ISSN: 1545-9624 (Print) 1545-9632 (Online) Journal homepage: http://www.tandfonline.com/loi/uoeh20

Performance of a Scanning Mobility Particle Sizer in Measuring Diverse Types of Airborne Nanoparticles: Multi-Walled Carbon Nanotubes, Welding Fumes, and Titanium Dioxide Spray

Bean T. Chen, Diane Schwegler-Berry, Amy Cumpston, Jared Cumpston, Sherri Friend, Samuel Stone & Michael Keane

To cite this article: Bean T. Chen, Diane Schwegler-Berry, Amy Cumpston, Jared Cumpston, Sherri Friend, Samuel Stone & Michael Keane (2016): Performance of a Scanning Mobility Particle Sizer in Measuring Diverse Types of Airborne Nanoparticles: Multi-Walled Carbon Nanotubes, Welding Fumes, and Titanium Dioxide Spray, Journal of Occupational and Environmental Hygiene, DOI: 10.1080/15459624.2016.1148267

To link to this article: http://dx.doi.org/10.1080/15459624.2016.1148267

Accepted author version posted online: 12 Feb 2016.

Performance of a Scanning Mobility Particle Sizer in Measuring Diverse Types of Airborne Nanoparticles: Multi-Walled Carbon Nanotubes, Welding Fumes, and Titanium Dioxide Spray

Bean T. Chen, Diane Schwegler-Berry, Amy Cumpston, Jared Cumpston, Sherri Friend, Samuel Stone, and Michael Keane

Health Effects Laboratory Division, National Institute for Occupational Safety and Health, Morgantown, West Virginia

Address correspondence to: Bean T. Chen, Health Effects Laboratory Division, National Institute for Occupational Safety and Health, 1095 Willowdale Rd., Morgantown, WV 26505-2888, USA; e-mail: bdc4@cdc.gov

Keywords: Nanoparticles, Direct-Reading Instrument, Multi-Walled Carbon Nanotubes, Welding Fumes, Titanium Dioxide, Real-Time Monitoring

Word Count of the Exposition: 6020

ABSTRACT

Direct-reading instruments have been widely used for characterizing airborne nanoparticles in inhalation toxicology and industrial hygiene studies for exposure/risk assessments. Instruments using electrical mobility sizing followed by optical counting, e.g., scanning or sequential mobility particle spectrometers (SMPS), have been considered as the "gold standard" for characterizing nanoparticles. An SMPS has the advantage of rapid response and has been widely used, but there is little information on its performance in assessing the full spectrum of nanoparticles encountered in the workplace. In this study, an SMPS was evaluated for its effectiveness in producing "monodisperse" aerosol and its adequacy in characterizing overall particle size distribution using three test aerosols, each mimicking a unique class of real-life nanoparticles: singlets of nearly spherical titanium dioxide (TiO_2), agglomerates of fiber-like multi-walled carbon nanotube (MWCNT), and aggregates that constitutes welding fume (WF). These aerosols were analyzed by SMPS, cascade impactor, and by counting and sizing of discrete particles by scanning and transmission electron microscopy. The effectiveness of the SMPS to produce classified particles (fixed voltage mode) was assessed by examination of the resulting geometric standard deviation (GSD) from the impactor measurement. Results indicated that SMPS performed reasonably well for TiO_2 (GSD = 1.3), but not for MWCNT and WF as evidenced by the large GSD values of 1.8 and 1.5, respectively. For overall characterization, results from SMPS (scanning voltage mode) exhibited particle-dependent discrepancies in the size distribution and total number concentration compared to those from microscopic analysis. Further investigation showed that use of a single-stage impactor at the SMPS inlet could distort the size distribution and underestimate the concentration as shown by the SMPS, whereas the presence of vapor molecules or atom clusters in some test aerosols might cause artifacts by counting "phantom particles." Overall, the information obtained from this study will help understand the limitations of the SMPS in measuring nanoparticles so that one can adequately interpret the results for risk assessments and exposure prevention in an occupational or ambient environment.

INTRODUCTION

Aerosols containing nanoparticles are present in nature (e.g., volcanic smoke, cloud condensation nuclei, and airborne viruses) and have been traditionally classified as the ultrafine fraction of airborne particulates. In contrast to nanoparticles produced in nature, man-made nanoparticles can be present as incidental aerosols, such as welding fume in a workplace, diesel exhaust in ambient air, and side-stream cigarette smoke in an indoor environment, or be synthesized during the manufacturing process of nanomaterials, such as carbon nanotubes, nano-titanium dioxide, or silver nanowires. With the dramatic growth of nanotechnology, there are concerns about potential health risks of these man-made nanoparticles; they have the unique properties of possessing a large specific surface area to enhance the reactivity on cellular surfaces as well as maintaining a small size to allow potential translocation across cellular barriers.[1,2] Nanoparticles, especially those engineered ones, are commonly defined based on the smallest single unit of the nanomaterial, and have at least one dimension between 1 and 100 nm.[3] This definition can sometimes be confusing because the actual dimension(s) of a nanoparticle (e.g., the length of a carbon nanotube or the size of titanium-dioxide agglomerate) is typically micrometers rather than nanometers. Airborne nanoparticles have a diverse range of shapes and morphologies, ranging from spherical nano-titanium dioxide,[4] to inhomogeneous aggregates of spheres, such as welding fume,[5] and particle agglomerates such as those composed of fiber-like carbon nanotubes.[6]

Direct-reading aerosol instruments have often been used for near-real-time aerosol measurements in ambient air and workplace environments.[7] With the growth of nanotechnology, those types of instruments, especially those focused on number-based

measurement, have frequently been used for concentration measurements and size distribution of airborne nanoparticles, although no scientific consensus exists yet for the most appropriate exposure metric for nanoparticles. The fast response and good counting statistics make direct-reading instruments very convenient, especially compared with mass-based sample collection methods that may require extensive preparation and tend to have low sensitivity for nano-sized fractions. The instruments, however, rely on indirect techniques to create electronic signals from particle sensing, and thus calibration is required by the manufacturer. Accuracy of instrument calibration depends on the relationship between signals in a sensing zone and the aerosol properties; [8] this relationship is based on an empirical model of the instrument response to monodisperse test particles (generally spherical shape) of known concentration. The limitations of this approach is that if the aerosol under study is significantly different in properties from that used in the manufacturer's calibration then the calibration may no longer be valid and consequently erroneous measurements will occur with the instrument.

Among the instruments, those using an electrical mobility sizing scheme combined with a condensation nuclei counting technique, such as a scanning or sequential mobility particle spectrometer (SMPS), have been widely used and have been proposed as one of the standard instruments for measuring nanoparticles by international agencies.[9,10] Although the instruments have been used for measuring nanoparticles of spherical shape, there is lack of information on their performance on nanoparticles of anisometric shapes.

To fill this gap, the overall goal of the study was to use diverse types of real-life airborne nanoparticles to examine the potential effects of particle shape, morphology and other physical properties on the performance of a commercially available SMPS. The specific aims and

methods to achieve this goal were to (1) develop three aerosol generation systems capable of producing 3 test nanoparticles with a diverse range of shape structure and morphology, (2) investigate the SMPS capabilities to produce near monodisperse test aerosols in fixed voltage mode by comparison to cascade impactor results, and (3) evaluate the SMPS performance by comparing the total number concentration and particle size distribution of test aerosols using microscopic analysis with those in the SMPS display under scanning voltage mode. The information obtained from this study will help understand the capabilities and limitations of the instrument in measuring airborne nanoparticles so that results can be interpreted for potential human risk assessments as well as exposure prevention in an occupational or ambient environment.

METHODS

Test Aerosols

Three types of nanoparticles were used in the present study: spray-can titanium dioxide (TiO_2) spheres, irregularly-shaped welding fume (WF) aggregates, and fibrous multi-walled carbon nanotube (MWCNT) agglomerates. They were selected because they represent real-life aerosol particles occurring in an indoor household or occupational environment as well as in an ambient atmosphere with a diverse range of shape structure and particle morphology. The aerosols were generated from three distinct systems [Figure 1] and have been used in animal inhalation facilities for nanotoxicological studies.[5,11,12] The systems are described in detail in Appendix A.

SMPS

Several SMPS are commercially available. In the present study, the TSI SMPS (Model 3936, TSI, Inc., Shoreview, MN) was used because of its availability. The instrument consists of a single-stage impactor (with a cutoff diameter around 0.5-0.7 μm), a bipolar ion source, a differential mobility analyzer (DMA; Model 3081), and a condensation particle counter (CPC; Model 3775). The impactor removes from the aerosol large particles that may carry multiple charges during bipolar charging and cause data inversion problems. The ion source neutralizes the aerosol to achieve the Boltzmann equilibrium charge distribution on the particles. The DMA then classifies positively-charged particles with a narrow range of electrical mobility by adjusting the voltage on the central rod of the analyzer. These classified particles exit through the DMA monodisperse aerosol outlet and are considered as "monodisperse" in size. Finally, by monitoring the exit aerosol with a CPC, the number concentration in each narrow range of mobility can be determined and consequently the overall size distribution of characterized aerosol particles can be constructed. In the present study, the SMPS was evaluated for 3 test aerosols based on the following requirements: (1) the DMA provides multiple monodisperse aerosol fractions, (2) each fraction is confirmed to have the expected size range, and (3) the overall size distribution and number concentration of each test aerosol is compatible with the data from microscopic analysis. The details of operating parameters used in the SMPS are described in Appendix B.

Experimental Setup and Operation

Figure 2 shows the schematic diagrams of two experimental setups used in the study: (A) is for examining the monodispersity of the DMA-classified aerosol particles using two micro-

orifice uniform-deposit cascade impactors (MOUDI Models 110 and 115; MSP Corp., Shoreview, MN) in tandem [the first part], and (B) is for comparing the total number concentration and particle size distribution of particles determined by the SMPS with those collected on filters followed by electron microscopic analysis [the second part]. For each test aerosol, the mass concentration in the sampling chamber was continuously monitored using a Data RAM (DR-40000 Thermo Electron Co, Franklin, MA). Once a stable concentration was established, the aerosol was then introduced into the SMPS for the experiment. The mean mass concentration, M_c, measured by the Data RAM was calibrated daily by taking samples using two 37-mm polytetrafluoroethylene filters (PTFE, 0.45 μm pore size, SKC Inc., Eighty Four, PA) from the chamber as described before.[4,5,6,11] For each aerosol only one concentration was used to check SMPS' performance except for MWCNT, in which two different mass concentrations were generated in the second part of the study to examine if varying concentration would alter particle morphology and consequently affect SMPS' performance.

In the first part of the study [Figure 2(A)], the DMA in the SMPS was operated at a fixed voltage mode to allow the production of "monodisperse" particles of a desired size range at the exit of the DMA. The CPC was bypassed in this setup; instead, the MOUDI with polycarbonate filters (Whatman, Clinton, PA) and microscopic grids as collection substrates was connected to the DMA to characterize the size of the classified nanoparticles. For each aerosol, several full SMPS scans, which were highly reproducible, were first acquired to ensure that the test aerosol had a steady peak size and a sufficient total number concentration prior to operating a fixed voltage mode. Three fixed voltages (or sizes) were selected in the DMA to extract three respective "monodisperse" aerosol fractions for MOUDI analysis. In the second part of the study

[Figure 2(B)], the SMPS was operated at a normal scanning voltage mode with both the DMA and CPC in place to characterize the overall aerosol passing through the single-stage impactor. For serial comparison with SMPS results, 47-mm polycarbonate filters (Whatman) of 0.1 μm pore size, one at a time, were intermittently installed between the impactor and the DMA to collect the aerosol that had been characterized by the SMPS. They were used to ensure the sampling of nanoparticles at a collection efficiency of ≥99%[13] for adequate characterization of test aerosols for comparison. Detailed operating procedures for the study are described in Appendix C.

Data Analysis

In the first part of the study, the size distribution associated with the DMA's classification was represented by the mean, D_{DMA}, shown in the DMA display with a range of ΔD_{DMA}, calculated based on the electrical mobility equivalent particle size width in Appendix C.[14,15] In the MOUDI, the filters and the grids from each impaction stage were prepared for microscopic analysis. The particles on the filter samples were viewed using a field emission scanning electron microscope (FE-SEM; Hitachi, S-4800, Tokyo, Japan) and those in the grid samples were observed through a JEOL 1220 transmission electron microscope (TEM, JEOL Inc., Tokyo, Japan). The particles in a representative sample of the filter (not those on the grid) of each stage were counted; each discrete particle or particle structure was counted as unity. The information was then numerically fitted with the corresponding cutoff size of the stage to determine the particle size distribution using a data inversion method.[16] The geometric mean, D_{MOUDI}, and the geometric standard deviation, GSD, were then compared to $D_{DMA,}$ and ΔD_{DMA} obtained from DMA classification.

In the second part of the study, the filter samples were analyzed using the FE-SEM by counting and sizing of discrete particles on the samples. For sizing, the geometric equivalent diameter based on the microscopic measurement of particle geometry, D_M, is used as a metric for presenting the size distribution of the aerosol. For particle counting, the procedures described previously were followed to determine the mean number concentration (i.e., N_{MIC}), which was then compared to the mean value from SMPS (designated as N_{SMPS}) using t-tests. In addition, the relative number of particles in selected size intervals was used to characterize the size distribution, presented by D_{MIC} and GSD. They were then compared with the size distribution in the statistics table of SMPS (designated as D_{SMPS} and GSD) using 95% confidence intervals for the geometric mean. The details of data analysis are described in Appendix D.

RESULTS

Generation of Test Aerosols

Three distinct systems were used for the generation of test aerosols [Figure 1]. The mass concentrations of TiO_2, MWCNT, and WF aerosols in the chamber were respectively maintained at 4.8, 6.5, and 4.5 mg/m^3 during the first part of the study [Table I] and remained steady at 5.2, 7.4, and 4.1 mg/m^3 during the second part of the study [Table II]. As described previously, an additional concentration of MWCNT at 0.5 mg/m^3 was used in the second study. The electron photomicrographs of particles in the test aerosols are also shown in the figure, which exhibit diverse morphologies with unique structures: (A) singlet spheres of TiO_2 spray particles, (B) agglomerates of MWCNT fiber-like particles, and (C) aggregates of WF spheres.

Investigation of DMA-Classified Test Aerosols Using MOUDI

Table I presents the results from the first part of the study, in which each DMA-classified test aerosol was characterized by comparing its electrical mobility equivalent size distribution based on the operational settings made in the DMA to the aerodynamic equivalent size distribution determined using the MOUDI. For each test aerosol, three different fixed voltages were selected in the DMA to generate three size-fractionated particles at the monodisperse aerosol outlet for comparison. This is to examine the effectiveness of SMPS in producing monodisperse nano-sized aerosol particles. The mean size (D_{DMA}) and size range (ΔD_{DMA}) estimated from each applied voltage and associated electrical mobility are presented in the table along with D_{MOUDI} and GSD determined from counting of discrete particles present on the MOUDI stages of different cutoff sizes. The table shows three major results: comparisons of "monodispersity," comparisons of mean particle sizes, and general correspondences between the SMPS data and the MOUDI results.

For monodispersity, the SMPS results indicate that all of the fractionated aerosols at the DMA monodisperse aerosol outlet had a relatively narrow particle size width (ΔD_{DMA}) with respect to D_{DMA}, as evidenced by a narrower ΔD_{DMA} for a smaller D_{DMA}. The MOUDI results, however, show that the sizes of the fractionated particles were quite spread out and appeared on multiple stages (4-7 stages) in the impactor with a wide range of GSD values (1.31-1.78), depending on the type of nanoparticles and the size of fractionation (D_{DMA}). The GSD is a conventional index of the spread of particle sizes and GSD values $\leq$1.22 are associated with monodisperse aerosols;[17] those (1.31-1.32) found for TiO_2 are close to this criterion, but not those (1.45-1.78) found for MWCNT and WF.

For the mean size comparisons (D_{DMA} vs. D_{MOUDI}), all MOUDI results for WF were less than the expected size from SMPS, while the opposite seemed to be true for TiO_2 except that no particles in the 50-nm size fraction were observed in MOUDI samples.

In terms of general correspondences between SMPS and MOUDI, results reveal that, for TiO_2 in the 50-nm size fraction, no actual corresponding particles were seen on any MOUDI stages. This discrepancy will be addressed in the Discussion section.

For each of the DMA-classified test aerosols, a representative set of samples collected on the different MOUDI impactor stages is shown in Figure 3 to complement the results in Table I: (A) SEM images of classified MWCNT particles (D_{DMA} = 350 nm); (B) TEM images of WF particles (D_{DMA} = 300 nm); and (C) SEM image of TiO_2 particles (D_{DMA} = 160 nm).

Characterization of Overall Test Aerosols

Morphological Analysis of Nanoparticles

In the second part of the study, test aerosols passing through the SMPS were intermittently collected on filters and then the discrete particles were counted and sized using the FE-SEM for subsequent comparison with SMPS data. Table II lists the general information on the samples analyzed via the FE-SEM. Among the three test aerosols, TiO_2 samples consisted primarily of individual spherical nanoparticles (96% in number) with little particle coagulation. The smallest and the largest particles were 44 nm and 895 nm, respectively, with the mode of the distribution around 89 nm. WF samples contained mainly chain and clustered aggregates of metal oxide spheres, with 8% of the particles containing <10 spheres. The average number was 240 spheres per aggregate with the most probable size of a sphere around 26 nm. Results also indicate that only 3% of the particles were singlets with the smallest size of 49 nm. In the case of

MWCNT samples, the single-stage impactor seemed to remove a large portion of particles from the input aerosol, especially those containing highly-agglomerated nanotubes. This phenomenon was clearly illustrated by comparing the number of nanotubes per particle between this study (geometric mean of 5.7 and 6.3) and the previous study (geometric mean of 16) which collected samples without the use of an impactor.[6] In addition, data indicated minor differences between the two MWCNT concentrations (0.5 vs. 7.4 mg/m^3) in terms of number of fibers per particle, fibrous particle fraction, aspect ratio, and overall length and width range of the particles. It is, however, evident that particle morphology can be very different among the 3 test aerosols.

Comparison between SMPS Data and Microscopic Measurements

Test aerosols passing through the SMPS were characterized for number concentration based particle size distributions. The graphic and numeric results from the counting and sizing of discrete nanoparticles using the FE-SEM were compared with those directly from the SMPS printout under the scanning voltage mode. Figure 4 illustrates the number concentration-based particle size distributions obtained from the SMPS display (A) and the microscopic measurement (B). The SMPS displays exhibit abrupt truncation at both size edges, whereas the histograms obtained from microscopic measurements tend to be smooth and continuous around the boundaries. This phenomenon is expected since SMPS has an internal algorithm to impose the upper (0.5 μm) and lower (11 nm) size measurement range, and ideally the upper size should correspond well to the D_{50} (50% cutoff diameter; = 0.5 μm) of the single-stage impactor. By comparing the corresponding distributions for each test aerosol in Figure 4, the discrepancy between the two measurements seems to be most significant in the region around and greater than the upper size limit (500-1000 nm) and the degree of bias depends on the complete size

distribution of the test aerosol (upstream of the impactor) relative to the D_{50} (or, how large a fraction of the actual size distribution was chopped off).

Data in Figure 4 are presented numerically in Table III for comparison of total number concentration (N_{SMPS}) and size distribution (D_{SMPS} and GSD) determined by SMPS to the corresponding number concentration (N_{MIC}) and size distribution (D_{MIC} and GSD) quantified from the filter samples. Unimodal continuous distribution models were fitted for the discrete data from both the SMPS and microscopic counting and sizing methods, and the resulting distributions were compared using established tests.[18] The table indicates that N_{MIC} was greater than N_{SMPS} for MWCNT and TiO_2, but the two were about the same for the WF. For the size distribution, D_{MIC} was larger than D_{SMPS} for all the test aerosols, with the highest discrepancies applying to MWCNT. In addition, MWCNT of a lower mass concentration did possess a lower number concentration with a slightly smaller mean size. The table also presents evidence of statistical difference between the two number concentrations (N_{SMPS} vs. N_{MIC}) using t-test results. The 95% confidence intervals (CI) for the mean (D_{SMPS} vs. D_{MIC}) were used for showing the difference between the two size distributions.

Another form of number concentration and size data from the SMPS is also reported in Table III in square brackets. The data were obtained by applying an adjustment to correct for multiple charge distribution on the particles.[19] Generally, the adjusted data show a larger D_{SMPS} with a lower N_{SMPS} compared to those obtained for the non-adjusted data.

DISCUSSION

Data indicate that SMPS results are influenced by particle shape and morphology, as well as by the the upper and lower size limits set by the instrument. These influences affect

SMPS' performance in particle classification, detection, and data registration and, consequently, have implications for exposure assessment and toxicology studies that rely on SMPS as gold standard measurement.

Performance of Electrical Classification of Nanoparticles

Effectiveness of Electrical Classification of Test Nanoparticles

Table I indicates that the classified TiO_2 aerosols were reasonably monodisperse, based on MOUDI results, with GSDs of 1.31-1.32, which is close to the criterion of ≤ 1.22[17] for monodispersity. In the case of WF, results were far from monodisperse, with GSDs ranging from 1.45 to 1.56. In Figure 3(B), images of stages 6-12 show that the DMA-classified WF particles (having a similar electric mobility) were not deposited on a single stage (or merely on adjacent stages) of the impactor as expected for a monodisperse aerosol; they appeared on seven stages of the impactor (having different aerodynamic diameters). This shows a substantial difference in the particle aerodynamic diameters as measured by the MOUDI relative to a 350-nm diameter "monodisperse" fraction of WF aerosol as classified according to electrical mobility diameter by SMPS. Likewise, the diverse range of particle size and morphology in 3(B) shows considerable variation in the particle geometric diameters for the same electrically fractionated WF aerosol. Similar findings applied to MWCNT aerosols, with large GSDs of 1.57-1.78, and wide particle distribution on the MOUDI stages. MWCNTs in Figure 3(A) contain isometric, fibrous, and irregularly-shaped particles. This discrepancy between the electrical and the aerodynamic (and geometric) classification was expected for MWCNT and WF because the electrical charge distribution for nanoparticles containing anisometric agglomerates or aggregates can be very different from those based on singly-charged spherical particles used in the SMPS algorithm.

This phenomenon occurs because the electrical mobility of a fibrous particle depends heavily on the length whereas its aerodynamic behavior is more associated with the width.[20] As a result, particle electrical mobility and aerodynamic size would not necessarily have the unique correspondence required for an ideal "monodisperse" distribution. Compared to WF and MWCNT, the discrepancy is much less for TiO_2 [Figure 3(C)], suggesting that the discrepancy may be largely associated with particle shape and morphology, and that aerosols containing nanoparticles of spherical singlets do possess a narrow range of particle size distribution following the electrical classification by DMA.

D_{MOUDI} vs. D_{DMA}

Besides the particle scattering phenomenon described above, Table I shows that D_{MOUDI} values are different from the corresponding D_{DMA} values and the degree of discrepancy depends on the type of test nanoparticles. The difference of these two values was expected because particle aerodynamic diameter (a function of effective density, shape factor, etc.) is fundamentally different from its electrical mobility diameter (a function of dielectric constant, number of electric charge, etc.). However, the variations of the values among the three classifications within a given test aerosol may reveal additional information concerning the effectiveness of electrical technique in classifying the type of nanoparticles. For MWCNT, classified aerosol of very different D_{DMA} (180, 350, and 450 nm) have similar corresponding D_{MOUDI} values (285, 301, and 314 nm), indicating that electrical classification was not very effective in separating MWCNT fibrous particles according to particle aerodynamic behavior or equivalent geometry and, as a result, all three DMA-classified aerosols contained relatively similar D_{MOUDI} values with most particles deposited on the 8th stage of the MOUDI. This poor

resolution in aerodynamic and geometric size distribution for the three DMA-classified MWCNT aerosols can be associated with the complex shape and structure of nanotubes and their agglomerates, which influenced the charge distribution on the particle during bipolar charging and the drag on the particle during electrical classification in the DMA. Therefore, their actual mobilities are different from those predicted for spheres of an equivalent geometry as used in the SMPS algorithm, and, as a result, effective classification does not hold well for test nanoparticles such as MWCNT. This effect, however, appears to be less significant for irregularly-shaped WF aggregates in which particles of different D_{DMA} values (100, 180, and 300 nm) exhibited different corresponding values of D_{MOUDI} (83, 150, 182 nm) [Table I], indicating that electrical classification did provide reasonable geometric size separation of particles with different aerodynamic behavior. It is, however, interesting to find that, different from MWCNT, WF shows smaller D_{MOUDI} values than the corresponding D_{DMA} values. In the absence of detailed knowledge, this effect may be partly related to the aerodynamic behavior of plane-shaped WF particles containing chain/cluster aggregates in an impactor, in which disc-like particles exhibit a smaller aerodynamic diameter than spheres with equivalent geometry.[21] In the case of TiO_2 spheres, the effect of particle shape is disregarded and the differences between D_{MOUDI} and D_{DMA} can be related to particle density and slip correction between their aerodynamic and geometric diameters under the assumption of singly-charged particles.

Phantom Particles

Table 1 shows that, in the case of the classified TiO_2 aerosol with D_{DMA} = 50 nm, no particles could be seen on any of the filter samples using FE-SEM, even though the SMPS' display showed a considerable concentration of particles in the 50-nm size fraction. Although

this discrepancy cannot be clearly explained, it was possible that the SMPS signals were activated by the transient presence in the CPC of DMA-classified positively-charged vapor molecules created by the propellant during spray can operation, even though no TiO_2 particles were actually present in the DMA-classified aerosol stream (ΔD_{DMA} = 49-52 nm). Therefore, this discrepancy is considered as an artifact ("phantom particles") of the SMPS data. Note that this is only a proposed reason to explain this finding and no detailed proof can be provided at this time. Nevertheless, it is suggested that thorough examination and careful interpretation be required when nanoparticles are characterized using a SMPS, showing ultra-nano size distribution such as that in the spray can aerosol products under special formulation. This issue will be discussed later when comparing the number concentration and particle size distribution of test nanoparticles.

Particle Size Distribution and Number Concentration: SMPS Display vs. Microscopic Analysis

The SMPS was also operated under an ordinary scanning voltage mode to characterize each of the test aerosols and the results were compared to those using microscopic measurements. As mentioned before, the aerosol analyzed by SMPS did not represent a complete sample of aerosol particles at the inlet, but only those able to pass through the single-stage impactor, into the DMA, and detected by CPC. Consequently, this results in a SMPS display (under a maximum view format) with a cutoff (or truncation) on both edges of the particle size distributions (D_p = the electrical mobility diameter) [Figure 4(A)].

Effects of Cutoff Edge in the SMPS Display

Besides the SMPS displays in 4(A), Figure 4(B) shows the corresponding number-based size distributions determined from microscopic measurements of D_M, the geometric equivalent diameter. In contrast to the abrupt truncation in the right edge of the SMPS displays, these histograms illustrate a relatively smooth profile around the upper size bound. This discrepancy is evident because, even though the upper size limit of the SMPS is set at D_{50} (50% cutoff), some particles $>D_{50}$ can still pass through the impactor as part of the test aerosol. Although these $>D_{50}$ discrete particles were sized and counted as particles larger than the upper size limit as shown in the microscopic analysis [4(B)], they were size-constrained in the SMPS and considered either as particles $<D_{50}$ or not even registered as particles in the SMPS display [4(A)], depending on the charge polarity and the electrical mobility of each particle. Similarly, some particles $<D_{50}$ can be removed by the impactor and result in a decrease of total number concentration. With this in mind, the results from the microscopic analyses [Figure 4 and Table III] of the overall aerosol samples show a general trend of smoother size distributions around the upper size limit with a higher number concentration and a larger geometric means size compared to those from the SMPS displays. In addition, quantitative analyses indicate that the degree of differences between SMPS results and microscopic measurements may be attributed to the differences in morphology, density, and electrical properties of the three distinct nanoparticles. For comparisons of number concentrations between the microscopic and SMPS data [N_{MIC} vs. N_{SMPS}], there is approximately two fold difference for MWCNT [2.51×10^3 vs. 1.00×10^3 #/cm^3 (low concentration) and 2.76×10^4 vs. 1.33×10^4 #/cm^3 (high concentration)], a small 28% difference for TiO_2 [1.40×10^5 vs. 1.01×10^5 #/cm^3], and an insignificant discrepancy for WF

[5.17 x 10^5 vs. 5.09 x 10^5 #/cm^3]. Results from t-tests showed that mean number concentrations were different for low-and high-concentration MWCNTs (p=0.002 and 0.001 respectively), and TiO_2 (p=0.004), but no significant difference was evident for WF. A similar trend of difference applies to the size distribution [D_{MIC} vs. D_{SMPS}] with the 95% CI for the geometric mean[18] did not overlap for all 3 test aerosols: (467, 517) vs. (275, 289) (high) and (399, 443) vs. (251, 301) (low) for MWCNT; (107, 123) vs. (94, 98) for TiO_2; and (186, 206) vs. (170, 172) for WF. Although the respective differences between (N_{MIC}, D_{MIC}) and (N_{SMPS}, D_{SMPS}) were expected for the anisometric nanoparticles such as MWCNT agglomerates, it was surprising to discover that no significant difference in the number concentration for the WF aggregates test aerosol. Without further investigation on the physical properties (e.g., charge distribution on the surface of an aggregate and its preferred orientation in an electric field) of the WF nanoparticles, it is difficult to explain why WF nanoparticles behave differently from MWCNT nanoparticles. Nevertheless, the results indicate that SMPS displays with a wide truncation at the right size edge tend to underestimate both the number concentration and mean particle size of the overall test aerosol; however, the degree of decrease depends on the type of test nanoparticles.

SMPS data adjusted using multiple charge corrections are also presented in square brackets of Table III. The corrected data bring about higher D_{SMPS} values but lower N_{SMPS} than those for the normal format, which seem to reduce the difference for the mean particle size (D_{MIC} vs. D_{SMPS}) but widen the discrepancy for the total number concentration (N_{MIC} vs. N_{SMPS}). Again, the 95% CI for the mean did not overlap for all 3 test aerosols, indicating the difference between the size distributions displayed by the SMPS and measured from the microscopic analysis.

Noting that the correction is based on the spherical particles with Boltzmann equilibrium charge distribution, it would not provide an adequate solution for particles with anisometric particles.

Overall, the information described above illustrates that, when using SMPS, test aerosols should not possess many particles larger than the upper size limit, or D_{50}, in the display. It is clear that a distorted SMPS size profile, as in the case of MWCNT nanoparticles, would not provide adequate information on the total number concentration and the particle size distribution whether operated under a normal or a corrected format.

Potential Artifacts in the Smaller Size Bins of the SMPS Display

Results from the TiO_2 samples show that the smallest particle size measured via FE-SEM was 44 nm [Table II], while the SMPS display illustrates that there were particles ≤40 nm with a mode around 18 nm [Figure 4(A)]. This discrepancy is similar to the artifact described in the first part of the study under the fixed voltage mode, in which the SMPS display indicated the presence of particles in the 50 nm size bin (ΔD_{DMA} = 49-52 nm; Table I), yet no particles could be actually observed in this classified sample through FE-SEM. Although this discrepancy cannot be clearly explained, it was considered as a result of "phantom particles." In contrast to the effect of abrupt truncation in the upper size of the SMPS display, this discrepancy adjacent to the lower size bound (~14 nm) would overestimate the overall number concentration of nanoparticles as well as shift the particle size distribution to the lower size range. In addition, the degree of discrepancy may depend on the properties of vapor constituents in the aerosol stream, such as the vapor concentrations, their saturation ratio and charge state. Despite an observable discrepancy in the case of TiO_2, the difference was minimal or nonexistent for WF and MWCNT. However, considering that the smallest WF particle observed was 49 nm [see Table II]

and SMPS display indicates the presence of particles <20 nm, this phenomenon of overestimation in number concentration of particles adjacent to the lower size bound may partially compensate for the underestimation in number concentration of particles around the upper size bound (~0.5 μm) and, as a result, the results were not very different between the SMPS (normal format) and microscopic measurements for the WF test aerosol. Nevertheless, the phenomenon affects primarily the small size bins of the SMPS display and, thus, this discrepancy would be important when using SMPS data for characterizing ultra-nanoparticles near or smaller than 20 nm.

CONCLUSIONS AND RECOMMENDATIONS

The results from the present study provide the following conclusions and recommendations that should be considered prior to using an SMPS:

(1) The size-fractionated samples based on a narrow electrical mobility classification from the electrostatic classifier were in some cases far from monodisperse with respect to their aerodynamic or geometric equivalent diameters. For spherical TiO_2 particles, size classification was reasonably effective and the classified aerosol had a narrow particle size range (GSD = 1.3). Size classification was generally poor for anisometric particles, such as WF aggregates and MWCNT agglomerates (GSD = 1.5-1.8). For fibrous particles, it is known that their electrical mobility depends on the length whereas their aerodynamic behavior is more associated with the width. However, for other irregularly-shaped particles there are a number of possible contributions to this: it is possible that the aerosol did not achieve Boltzmann charge equilibrium after passing through the neutralizer, due to an insufficient number of ion

collisions or other limitations of the device. In the case of WF, the fume aggregates are likely to have large charge excesses, from being generated at plasma conditions. Additionally, calculation expressions for electrical mobility are based on assumptions of point charges, while WF or MWCNT may have charge dispersion over the volume or surface of the nanoparticle structure, resulting in electrical mobilities that differ from those predicted by the model expression. Likewise, Stokes' terminal velocities are likely to differ strongly between spherical particles and the fiber-like MWCNT aggregates and also the WF aggregates. It is likely that all of these effects, and probably additional effects contribute to the lack of monodispersity for WF and MWCNTs. In brief, do not assume that DMA-classified aerosol of anisometric nanoparticles is monodisperse in size; therefore, caution is needed when using this aerosol for testing and calibration purpose.

(2) The "cutoff" phenomenon at the upper size bound of the SMPS display may create a discrepancy, i.e., particles greater than the size bound were present but not registered in the size distribution. Depending on the profile of the distribution, the discrepancy can be profound with a lower SMPS values in both number concentration and mean particle size (e.g., MWCNT), or less significant with a fractional reduction of SMPS values in number and size (e.g., TiO_2). It is highly recommended that the aerosol of interest have a complete size profile smaller than the upper size bound in SMPS display. For an aerosol containing a considerable fraction of particles larger than the upper size bound, an optical particle counter or an aerodynamic particle sizer should

be employed, in parallel with SMPS, to provide complementary data for a complete size distribution.

(3) Counts of "phantom particles" may be registered around the lower size bound of the SMPS display when, in fact, no particles exist in the classified aerosol stream. Results indicate this phenomenon applied to the TiO_2 test aerosol in both parts of the study, in which SMPS display showed the presence of particles whereas no actual particles were observed under FE-SEM. This finding indicates potential discrepancy in overestimating number concentration when using SMPS for characterizing ultra-nanoparticles (<20 nm). It is therefore recommended that SMPS data displays containing significant ultra-nanoparticles be supported with detailed photomicrograph images or other independent confirmations of the particles.

(4) Among the three aerosols tested, MWCNT nanoparticles were the most affected by the "cutoff" phenomenon on the upper size edge [see Table III; lower SMPS values in number concentration and particle size], while TiO_2 nanoparticles showed some discrepancies caused by the "phantom particles" [see Table I; potential overestimation of ultra-nanoparticles]. WF nanoparticles, however, presented a reasonably good agreement between the SMPS data and those using microscopic analysis [see Table III], even though this aerosol is supposedly affected by the "cutoff" phenomenon as discussed previously [see Figure 4]. At present, little is available to explicitly explain this agreement for WF nanoparticles. This clearly indicates that there is a pressing need concerning the information on charging mechanism and aerodynamic behavior of anisometric nanoparticles, such as cluster

aggregates and fiber agglomerates with various sizes, structures, and other physicochemical properties.

(5) The concept of electrical mobility-particle size relationship allows SMPS to be a useful tool for detecting submicron particles for qualitative monitoring (e.g., for evaluating the effectiveness of various control strategies), but can present problems when the device is employed for absolute quantitation of particle number concentration and size distribution (e.g., for assessing the workers' exposure dose for risk analysis). It is, thus, important to realize that the use of SMPS as measurement standard for aerosols containing anisometric nanoparticles is not recommended and the conventional use of filters and cascade impactor samples for characterizing aerosol concentration and size distribution are still the absolute standard for valid exposure analysis and adequate dose assessment of airborne nanoparticles. While the study was based on one specific SMPS, the results observed should be generalizable across all similar instruments.

ACKNOWLEDGMENTS

The authors would like to thank Mr. Howard Leonard, Mr. Walter McKinney, and Dr. Ali Afshari for their help and assistance with the aerosol generation and sample collection.

DISCLAIMER

The findings and conclusions in this article are those of the authors and do not necessarily represent the views of the National Institute for Occupational Safety and Health. The mention of any company names or products does not imply an endorsement by NIOSH or the Centers for Disease Control and Prevention, nor does it imply that alternative products are unavailable, or

unable to be substituted after appropriate evaluation. This article is not subject to US copyright law.

DECLARATION OF INTEREST

The authors report no conflicts of interest. The authors alone are responsible for the content and writing of the paper.

REFERENCES

1. **Oberdörster, G., V. Stone, and K. Donaldson:** Toxicology of nanoparticles: a historical perspective, *Nanotoxicology*. 1(1): 2-25 (2007).
2. **Kreyling, W.G., M. Semmler-Behnke, J. Seitz, et al.:** Size dependence of the translocation of inhaled iridium and carbon nanoparticle aggregates from the lung of rats to the blood and secondary target organs, *Inhal. Toxicol.* 21(S1):55-60 (2009).
3. **International Organization for Standards (ISO):** ISO TS 80004-1:2010 *Nanotechnologies - Vocabulary* - Part 1: Core Terms, Geneva, Switzerland: ISO, 2010.
4. **Chen, B.T., A. Afshari, S. Stone, et al.:** Nanoparticles-containing, spray can aerosol: characterization, exposure assessment, and generator design, *Inhal. Toxicol.* 22:1072-1082 (2010).
5. **Antonini, J. M., A. A. Afshari, S. Stone, et al.:** Design, construction, and characterization of a novel robotic welding fume generation and inhalation exposure system for laboratory animals, *J. Occup. Environ. Hyg.* 3:194-203 (2006).
6. **Chen, B.T., D. Schwegler-Berry, W. McKinney, et al.:** Multi-walled carbon nanotubes: sampling criteria and aerosol characterization, *Inhal. Toxicol.* 24:798-820 (2012).
7. **Pui, D.Y.H., and D.R. Chen:** Direct-Reading Instruments for Analyzing Airborne Particles. In *Air Sampling Instruments for evaluation of atmospheric contaminants 9th ed.*, B.S. Cohen and C.S. McCammon Jr. (eds.). Cincinnati, O.H.: ACGIH WORLDWIDE, 2001. pp. 377-414.
8. **Chen, B.T., R.A. Fletcher, and Y.S. Cheng:** Calibration of Aerosol Instruments. In *Aerosol Measurements: Principles, Techniques, and Applications 3rd ed.*, P. Kulkarni, P.

Baron, and K. Willeke (eds.). Hoboken N.J.: John Wiley and Sons, 2011. pp. 449-478.

9. **International Organization for Standards (ISO):** ISO 10808:2010 *Nanotechnologies* - Characterization of nanoparticles in inhalation exposure chambers for inhalation toxicity testing, Geneva, Switzerland: ISO, 2010.
10. **Organisation for Economic Co-Operation and Development (OECD):** Inhalation Toxicity Testing: Expert Meeting on Potential Revisions to OECD Test Guidelines and Guidance Document (Env/Jm/Mono (2012(14)), *Series on the Safety of Manufactured Nanomaterials No. 35.* Environment, Health and Safety Publications, Paris, France: OECD, 2012.
11. **McKinney, W., M. Jackson, T. M. Sager, et al.:** Pulmonary and cardiovascular responses of rats to inhalation of a commercial antimicrobial spray containing titanium dioxide nanoparticles, *Inhal. Toxicol.* 24(7):447-45 (2012).
12. **Porter, D.W., A.F. Hubbs, B.T. Chen, et al.:** Acute pulmonary dose-responses to inhaled multi-walled carbon nanotubes, *Nanotoxicology* 7(7):1179-1194 (2013).
13. **Liu, B.Y.H., D.Y.H. Pui, and K.L. Rubow:** Characteristics of Air Sampling Filter Media. In *Aerosols in the Mining and Industrial Work Environments,* B.Y.H. Liu and V.A. Marple (eds.). Ann Arbor, M.I.: Ann Arbor Science, 1983. pp. 989-1038.
14. **Flagan, R.C.:** Electrical Mobility Methods for Submicronmeter Particle Characterization. In *Aerosol Measurements: Principles, Techniques, and Applications 3rd ed.,* P. Kulkarni, P. Baron, and K. Willeke (eds.). Hoboken N.J.: John Wiley and Sons, 2011. pp. 339-364.

15. **Knutson, E.O., and K.T. Whitby:** Aerosol classification by electrical mobility: Apparatus, theory, and applications, *J. Aerosol Sci.* 6:443-451 (1975).

16. **O'Shaughnessy, P.T., and O.G. Raabe:** A comparison of cascade impactor data reduction methods. *Aerosol Sci. Technol.* 37:187-200 (2003).

17. **Mercer, T.T.:** *Aerosol Technology in Hazard Evaluation*, New York: Academic Press, 1973. p. 320.

18. **Silverman, L., C.E. Billings, and M.W. First:** *Particle Size Analysis in Industrial Hygiene*. New York: Academic Press, 1971. pp. 251-253.

19. **Wiedensohler, A. and H.J. Fissan:** Aerosol charging in high purity gases, *J. Aerosol Sci.* 19(7):867-870 (1988).

20. **Baron, P.A.:** Measurement of Asbestos and Other Fibers. In *Aerosol Measurement: Principles, Techniques, and Applications 1st ed.*, K. Willeke and P.A. Baron (eds.). New York: Van Nostrand Reinhold, 1993. pp. 560-590.

21. **Hinds, W.C.:** *Aerosol Technology - Properties, Behavior, and Measurement of Airborne Particles 2nd ed.*, New York: John Wiley and Sons, 1999. pp. 51-55.

22. **McKinney, W., B.T. Chen, and D. Frazer:** Computer controlled multi-walled carbon nanotube inhalation exposure system, *Inhal. Toxicol.* 21(12):1053-1061 (2009).

23. **Rodrigue, J., M. Ranjan, P.K. Hopke, and S. Dhaniyala:** Performance comparison of scanning electrical mobility spectrometers, *Aerosol Sci. Technol.* 41:360-368 (2007).

APPENDIX A: Test Aerosol Generation

Generation of TiO_2 Aerosols

Aerosols containing nano-sized TiO_2 particles were produced from a spray can aerosol generation system [Figure 1(A)].[4,11] The spray can product was provided and purchased on-line by the U. S. Consumer Product Safety Commission. It is marketed as containing "nano" TiO_2 particles and intended to be used as a surface antimicrobial agent, such as a bathroom sanitizer. In the system, a computer-controlled solenoid was used to push the bottom of the can upward to activate the aerosol spray. The spray can nozzle faced a direction opposite to the generator outlet to a sampling chamber [see Figure 2], which forced the impaction of large droplets on the flat surface by not following the 180° turn in the airstream and allowing only the TiO_2 nanoparticles to be able to negotiate the turn and exit on the upper right side of the generator. The reversal in the aerosol flow pattern was used to mimic exposure conditions of a user when applying the spray can product to a surface.[4] In addition, a mechanism combining an electromechanical clutch, a motor, and a gear box was computer-controlled to activate a 140° rotation of the spray can every 30 sec, mimicking frequent shaking of the can before and between sprays. Dry clean air was introduced into the system from the lower left side to ensure a good mixing of aerosol with resultant dry solid particles in the sampling environment downstream, while a drainage located at the lower region of the system allows excess fluid (droplets containing propellant) to be removed. The concentration of the aerosol was monitored in real time with a Data RAM (Thermo Electron) [see Figure 2] and feedback control was used to regulate the on/off time of the spray can activation and achieve a consistent concentration in the sampling environment. An electron photomicrograph of TiO_2 particles generated from this setup was shown in Figure 1(A).

Most particles were singlets with a spherical shape, indicating effective dispersion in the presence of propellant during spray can operation.

Generation of MWCNT Aerosols

Aerosols containing MWCNT particles were dispersed using an acoustical particle generation system [Figure 1(B)]. The nanotubes were catalytically grown by the chemical vapor deposition process and the bulk powder material provided by Mitsui & Co. (MWNT-7, lot 061220-31; Ibaraki, Japan) was placed inside the cylinder. In the system, acoustical energy generated by a speaker vibrated the top and bottom diaphragms of the generator in addition to the air column in the cylinder. The energy displaced the bulk material releasing particles and suspending them in the air. The constant air through the cylinder generated a flow pattern resembling that of a vertical elutriator and prevented coarse particles from leaving the cylinder. The aerosol contained respirable particles of individual fiber-like nanotubes and agglomerated nanotube structures with complex configurations.[6,22] In order to optimize the aerosol stability in the sampling chamber [Figure 2], a feedback control scheme like the one described above was used to maintain the desired, tightly controlled, aerosol concentration in the chamber. In the second part of the study MWCNT aerosols of two different concentrations were produced by adjusting the voltage in the speaker to examine if varying mass concentration would alter particle morphology and consequently affect SMPS' performance during comparison. Figure 1(B) shows the images of generated MWCNT particles collected on a filter. The particles contain mainly agglomerates with diverse morphologies of isometric, fibrous, and irregular shapes.

Generation of WF Aerosols

A two-room system divided by a UV-shielding curtain was used to produce WF aerosol for the study [Figure 1(C)]. In the system, a computer-controlled, robotic welder consisting of a power source, a robotic arm, a water-cooled welding torch, a wire feeder, and an automatic torch cleaner was developed to allow for continuous welding for extended periods of time without interruption.[5] The system was located in an enclosed, well-ventilated room adjacent to the control room where the equipment used for programming and monitoring the operation and performance of the welding system were housed. For the present study, gas metal arc welding was performed using a stainless steel electrode (Blue Max E308LSi wire; Lincoln Electric, Cleveland, Ohio). Welding was performed on A36 carbon steel plates (Huntington Steel, Morgantown, WV) at 25 V and 200 amps with a shielding gas of 95% argon and 5% CO_2 (Airgas Co., Morgantown, WV) at 20 L/min. The automatic feedback control like those described in the previous two generation/sampling systems was not used because the frequent start, stop, and cleanup steps of the welding process made it difficult, if not impossible, to maintain a stable fume particle concentration in the sampling chamber. Instead, the concentration was constantly monitored with a Data RAM and manually controlled by adjusting the dilution air in the system [Figure 2]. Figure 1(C) shows the morphology of the WF particles generated from the system. Most particles were aggregates in chains or clusters of primary spheres.

APPENDIX B: SMPS

Aerosol instruments that use the concept of voltage scanning, electrical mobility classification, and number counting for determining particle size distribution are commonly designated as the scanning or sequential mobility particle spectrometer (SMPS). They are

commercially available, such as the TSI scanning mobility particle sizer (TSI, Inc., Shoreview, MN), the GRIMM sequential mobility particle sizer (GRIMM Technologies Inc., Douglasville, GA), and the MSP wide-range particle spectrometer (MSP Corp., Shoreview, MN). In the present study, the TSI SMPS (Model 3936) was used because of its availability. The measurement of SMPS is based on the principles of steady-state bipolar equilibrium charging on submicrometer particles and subsequent electrical classification of singly-charged particles with a positive polarity. At the Boltzmann charge equilibrium, the percentage of particles of a given submicron size having the indicated mobility can be calculated.[19] Using this principle a unique electrical mobility is associated with every size of the classified particles and the classified particles are considered "monodisperse" [at the DMA monodisperse aerosol outlet] because of the narrow width in their mobility span. Hence, the entire particle size distribution of the aerosol characterized can be obtained by sequentially scanning through the voltage range. Because overall scanning normally requires several minutes, it is important to ensure a stable aerosol concentration during this time. In addition, aerosol flowrate should be carefully selected to be high enough to removes large particles from the aerosol in the impactor but low enough to provide sufficient residence time in the neutralizer to ensure particles achieving an equilibrium charge distribution.

SMPS measures the number concentration of aerosol particles. In the data display (under a maximum view format), it uses an internal algorithm to automatically select the lower (~10-12 nm) and the upper (0.4-0.6 μm) size measurement range based on the classifier flow rate at the smallest (-10 V) and the highest (-10 kV) scale of scanning voltages. While the lower size is related to the detection limit of the CPC, the upper size is associated with the 50% cut point (D_{50}

~0.5 μm) of the single-stage impactor installed in the SMPS to ideally pre-remove multiple-charged large particles prior to entering the DMA. To account for any potential presence of multiple-charged particles in the classified aerosol, the data of SMPS are presented in two formats: a normal format assuming particles with a single charge and a corrected format based on multiple-charges adjustment.[19] The function of this correction uses an internal algorithm that attempts to correct the sample data for the effects of multiple-charged particles, since the presence of more than one charge on a particle allows the particle to be incorrectly binned into a smaller-sized particle channel. Once activated, the SMPS program moves progressively from the upper size limit, D_{50}, to smaller size channels. In each size bin, the algorithm performs corrections by subtracting the number of multiple-charged particles from the number collected for the normal format.

SMPS has been widely used to generate monodisperse submicron aerosols using a fixed voltage mode and to measure airborne particles in the submicrometer size range using a scanning voltage mode.[14] It has been thoroughly investigated using test aerosols with spheres (e.g., polystyrene latex, dioctyl phthalate, oleic acid) and particles with well-defined shape (e.g., sodium chloride). In addition, dioctyl sebacate and carbon particles were used to conduct performance comparisons between the TSI SMPS and the MSP SMPS with reasonable agreements for particles in the range of 90-300 nm.[23]

APPENDIX C: Operating Procedures

Operating Procedures

Figure 2(A) shows the detailed setup for the first part of the study, in which the DMA was operated at a fixed voltage mode in the SMPS to allow “monodisperse” particles in a desired

size range exit via the monodisperse aerosol outlet of the DMA. The CPC, the particle detecting device in the SMPS, was bypassed in this setup; instead, the MOUDI with filters as the impaction substrates was installed downstream of the DMA to collect the classified aerosol particles for number-based particle size analysis. For each test aerosol, three fixed voltages (or sizes) were selected in the SMPS display prior to each run to extract three respective "monodisperse" aerosol fractions for MOUDI comparison. Several full SMPS scans were first acquired to ensure that the test aerosol had a steady peak size and a sufficient total number concentration. The peak size, along with two arbitrary sizes, one about one third smaller and the other about one third larger than the peak, were then selected, and their corresponding DMA voltages were calculated. The three corresponding voltages for the DMA were then used to produce three separate "monodisperse" fractions for size characterization using the MOUDI. To fulfill a 30 L/min total flow rate through the MOUDI, a makeup flow of clean air was introduced into the dilutor between the DMA and the MOUDI. Based on the number concentration shown in the profile (the peak was normally between $10^5 – 10^6$ particles/cm^3 in the SMPS), a sampling time ranging from 0.5 to 2 hours was determined for different fixed voltages. This was used as a guideline to provide a desired particle distribution of 0.02 particles per μm^2 substrate surface.[6] At the end of sample collection for each test aerosol, it is also important to run the overall size profile again using the scanning mode (with CPC) to confirm that the aerosol still maintained the same steady peak with sufficient number concentrations. For each monodisperse fraction of the test aerosol, a mean size (D_{DMA}) and an electrical mobility (Z_{EM}) were shown on the DMA front panel display and a mobility band (ΔZ_{EM}), and a particle size range (ΔD_{DMA}) can be calculated based on the voltage, flow rates, and geometry of the DMA.[14,15] The upper and lower sizes for

each ΔD_{DMA} can be calculated from the corresponding mobilities (i.e., Z_{EM} - ΔZ_{EM} and Z_{EM} + ΔZ_{EM}) in which $\Delta Z_{EM} = Z_{EM}$ x [sampling flow rate/sheath air flow rate].Figure 2(B) shows the setup for the second part of the study, in which the SMPS was operated at a normal scanning voltage mode with both DMA and CPC in place to size classify and characterize each segment of the aerosol and then present the total number concentration (N_{SMPS}) and particle size distribution (Geometric mean, D_{SMPS}, and geometric standard deviation, GSD) through the SMPS. The test aerosols examined by the SMPS were different from the complete aerosols from the generation system in that the aerosols characterized contained only those particles able to pass through the single-stage impactor at the inlet of the SMPS. Therefore, filter samples taken right after the single-stage impactor [Figure 2(B)] would be most representative and suitable for comparison with those characterized by the SMPS. To allow for serial comparison, a set of filter cassettes (one at a time) were intermittently installed between the single-stage impactor and the DMA to collect the aerosol that had been introduced into and characterized by the DMA. The filter collection was purposely arranged by utilizing the available airflow sensor in the SMPS so that the flow rate through the filter can be readily kept the same as that when no filter was installed. In this way, the 50% removal phenomenon in the impactor is the same with and without the filters so that aerosol samples collected on filters are adequate representatives of the overall aerosol through the system and, consequently, the total number concentration (N_{MIC}) and particle size distribution (geometric mean, D_{MIC}, and GSD) analyzed microscopically from the filters can be adequately compared with N_{SMPS} and D_{SMPS}/GSD. In this part of the study, the sampling flow rates were kept at 0.5 L/min so that the impactor has a 50% cutoff diameter around 0.5 µm. The sheath air was operated at 5 L/min to result in a lower size of 11 nm and an upper size of 0.5 µm

in the measurement range of SMPS. Again, a series of sampling time intervals between 0.5 and 30 minutes was chosen to achieve the optimal surface density of 0.02 particle/μm^2 on the filter.

APPENDIX D: Data Analysis

Real-Time Monitoring

The stable concentration M_c shown in the Data RAM was calibrated gravimetrically by taking two 37-mm PTFE filters (0.45 µm pore size; SKC) from the sampling chamber as described before.[4,5,6,11] The mass concentrations were calculated from the change in mass of the filter, airflow rate through the filter, and the sampling time. A balance (Mettler-Toledo, Model UMX2, Columbus, OH) with a resolution of 0.1 µg was used to measure filter weights.

Examining Mobility-Classified Samples under Fixed Voltage Mode

As depicted in Figure 2(A), a MOUDI was used to collect size-segregated samples of particles from 18 µm (cutoff diameter of the 1st stage) down to 10 nm (cutoff diameter of the 14th stage). Forty-seven-mm polycarbonate filters of 0.1 or 2.5 µm pore size (Whatman) each with a formvar coated electron microscopic grid attached at the center were used as the collection substrates. Prior to sampling, the filters were sputter-coated with a thin layer of gold/palladium (SPI-Module, Structure Probe Inc., West Chester, PA) for 20 sec at 20 mA to avoid undesired deposits on the sample due to electrostatic forces. In addition, this technique kept particles intact (no bounce or re-entrainment) on the filter surface even though no silicone oil spray was applied.[6]

After sampling, the microscopic grids were detached from the filters and the particles were directly viewed using a JEOL 1220 transmission electron microscope (TEM). The loaded

filters including the backup were each cut into four pieces and mounted onto aluminum stubs with double-stick carbon tape, and coated with gold/palladium using a SPI sputter coater. The samples were then analyzed using a field emission scanning electron microscope (FE-SEM; Hitachi). Because some MOUDI stages did not collect any particles, only the FE-SEM micrographs of the particles-containing samples were used for counting with appropriate magnifications between x5K and x20K. For each micrograph, fields of view over the entire effective sample area, including edge regions, were randomly selected. No overloading took place because the deposited particles were far apart from each other and approximately 30-300 particles were examined on each sample depending on its MOUDI stage relative to the peak of the size distribution. As described previously,[6] a particle structure, such as chain aggregate or clustered agglomerate, was counted as a single particle, rather than the number of individual objects forming the structure. The information on particle counts at corresponding stages was then numerically fitted to determine the particle size distribution, presented by the geometric mean, D_{MOUDI}, and the geometric standard deviation GSD, using a data inversion method by incorporating the actual stage collection efficiencies in the algorithm.[16] These values were then compared to the mean, $D_{DMA,}$ and the size width, ΔD_{DMA}, to examine the difference between aerodynamic diameter and electrical mobility diameter for each test nanoparticle, as well as the monodispersity of each DMA-extracted aerosol.

Characterizing Overall Aerosol Samples under Scanning Voltage Mode

In Figure 2(B), 47-mm polycarbonate filters (Whatman) of 0.1 μm pore size were used to ensure the sampling of nanoparticles before passing through the DMA at a collection efficiency of ≥99%.[13] The samples were then prepared as described in the previous section and analyzed

using the FE-SEM. An FE-SEM, rather than a TEM, was used to analyze the samples because the FE-SEM can provide size information concerning the 3-dimensional morphology of the particles examined. Conventional microscopic observations of particles deposited on a filter were used to provide direct measurements of the nanoparticles. Besides regular particle sizing and counting, the size and the number of primary particles in an aggregated or agglomerated particle structure were determined simultaneously by selecting a proper FE-SEM magnification in a representative area on the filter surface. For particle counting, the procedures described in the previous section were followed with suitable magnifications associated with the ability to detect particles in the aerosol sample. For sizing, the equivalent diameter based on the microscopic measurement of particle geometry, D_M, is used as a metric for presenting the size distribution of the test aerosols. It is defined as the diameter of a sphere that has the same compact geometry as the particle (including internal voids), similar to the projected area diameter defined for an anisometric particle when its 2-dimentional transmission electron microscopic image was used. While the value of D_M is straightforward to obtain for representing spherical or isometric particles such as TiO_2, it can be challenging to determine for anisometric particles, like WF aggregates or MWCNT fibers. In the present study, a set of procedures were followed to first portrait each WF aggregate or MWCNT fibrous particle as a compact cuboid and then present its volume equivalent sphere to determine the value of D_M. When viewing a particle via FE-SEM, a rectangle similar to the silhouette of the particle in compact form was visualized with a defined length (L) and width (W). Then, an approximation was considered to indirectly estimate the thickness (T) based on the most frequently appeared arrangement in the nanoparticle structures, in which fibrous MWCNT agglomerates were mostly configured by individual fibers bundled

together whereas WF aggregates were primarily organized via chain or cluster adherence of primary spheres. With this notion, the width W of each MWCNT particle was used to represent its thickness, whereas the square root ratio of projected area (i.e., L x W) to the number of the primary particles in each WF particle was considered as its thickness. D_M was then calculated as $(6/\pi \times L \times W \times T)^{1/3}$ for each anisometric particle. In the process all the information of a given particle and its primary singlet needs to be collected as a set even though a wide range of magnification is required for the different measurements. For example, FE-SEM magnifications of x7K – x15K were sufficient for measuring the length of MWCNT and WF particles, and TiO_2 particles >100 nm, whereas higher magnifications of x20K – x30K were needed for adequately assessing the width of individual MWCNT, the diameter of primary WF spheres and TiO_2 particles <100 nm.

For each micrograph, fields of view over the entire effective sample area were randomly selected for each filter. Approximately 600 particles were examined on each sample. The area on the filter to achieve a required particle number was used to determine the mean total number concentration (i.e., N_{MIC}), which was then compared to the mean value from SMPS (designated as N_{SMPS}). In addition, the relative number of particles in selected size intervals was used to characterize the particle size distribution, presented by D_{MIC} and GSD. They were then compared with the size distribution in the statistics table of SMPS (designated as D_{SMPS} and GSD). Both D_{SMPS} and D_{MIC} are presented as the geometric mean of the distribution. To provide a thorough comparison in this study, SMPS data were presented in two formats: a normal format assuming particles with a single charge, and a corrected format based on multiple-charges adjustment. In addition, numerous filter samples were collected for each test aerosol but only those having

similar D_{SMPS} and N_{SMPS} readings at pre- and post-filter collection were analyzed to provide needed statistical accuracy. For comparisons of number concentrations between the SMPS and microscopic data, t-tests were conducted using means, standard deviations and numbers of observations for each specific aerosol. The calculated p values less than 0.05 indicate significant differences in number concentration values. For comparison of difference between the two size distributions, a procedure[18] using 95% confidence intervals (CI) for the geometric mean was constructed to provide a measure of the range in which the true mean value is likely to lie. The criterion was set for two size distributions to be statistically different when there was no overlap between the two 95% CIs.

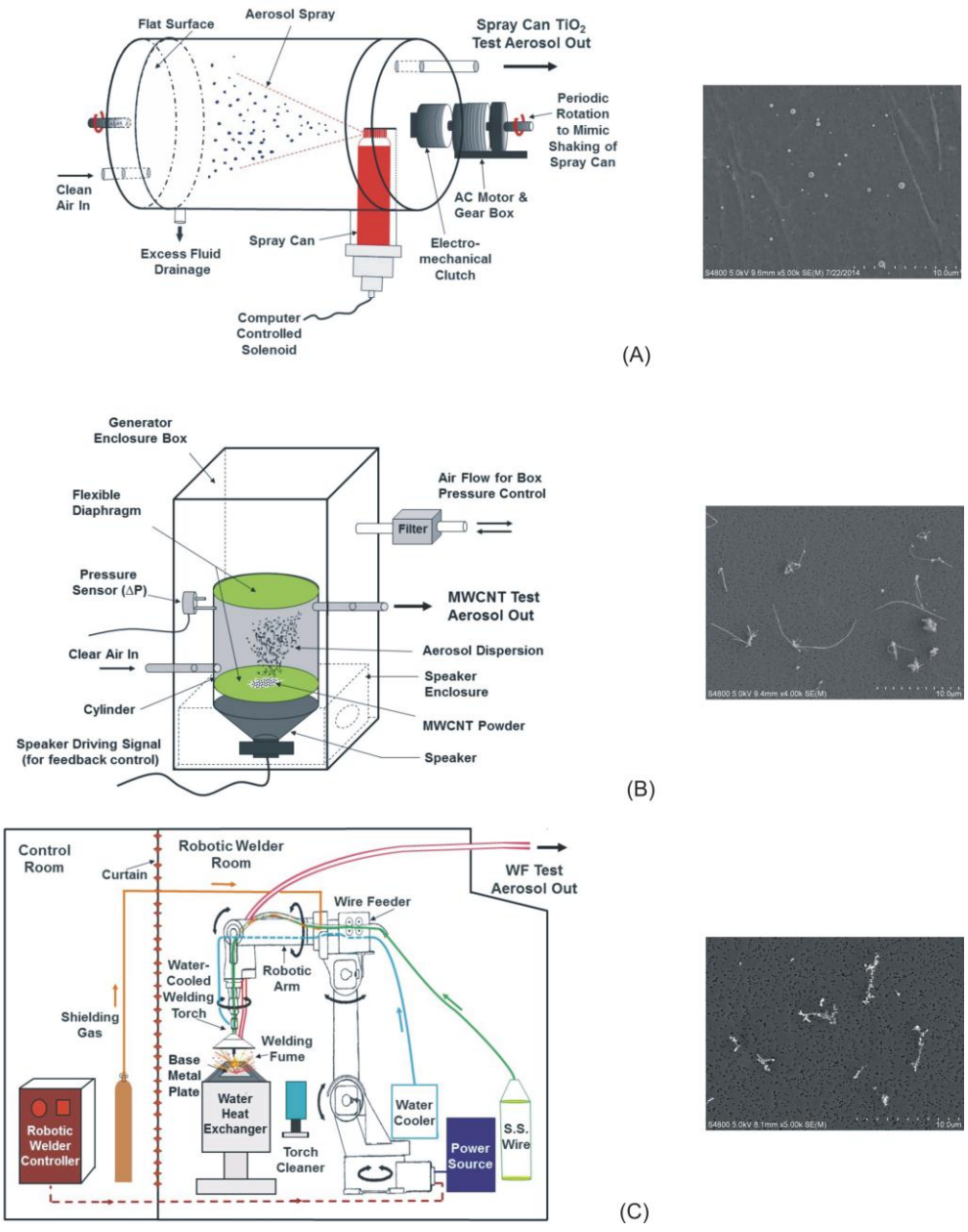

FIGURE 1. Aerosol generation systems used in the study: (A) spray-can titanium dioxide (TiO_2), (B) multi-walled carbon nanotubes (MWCNT), and (C) welding fume (WF). The corresponding images shown here were aerosol particles collected on 0.1-μm polycarbonate filters, respectively.

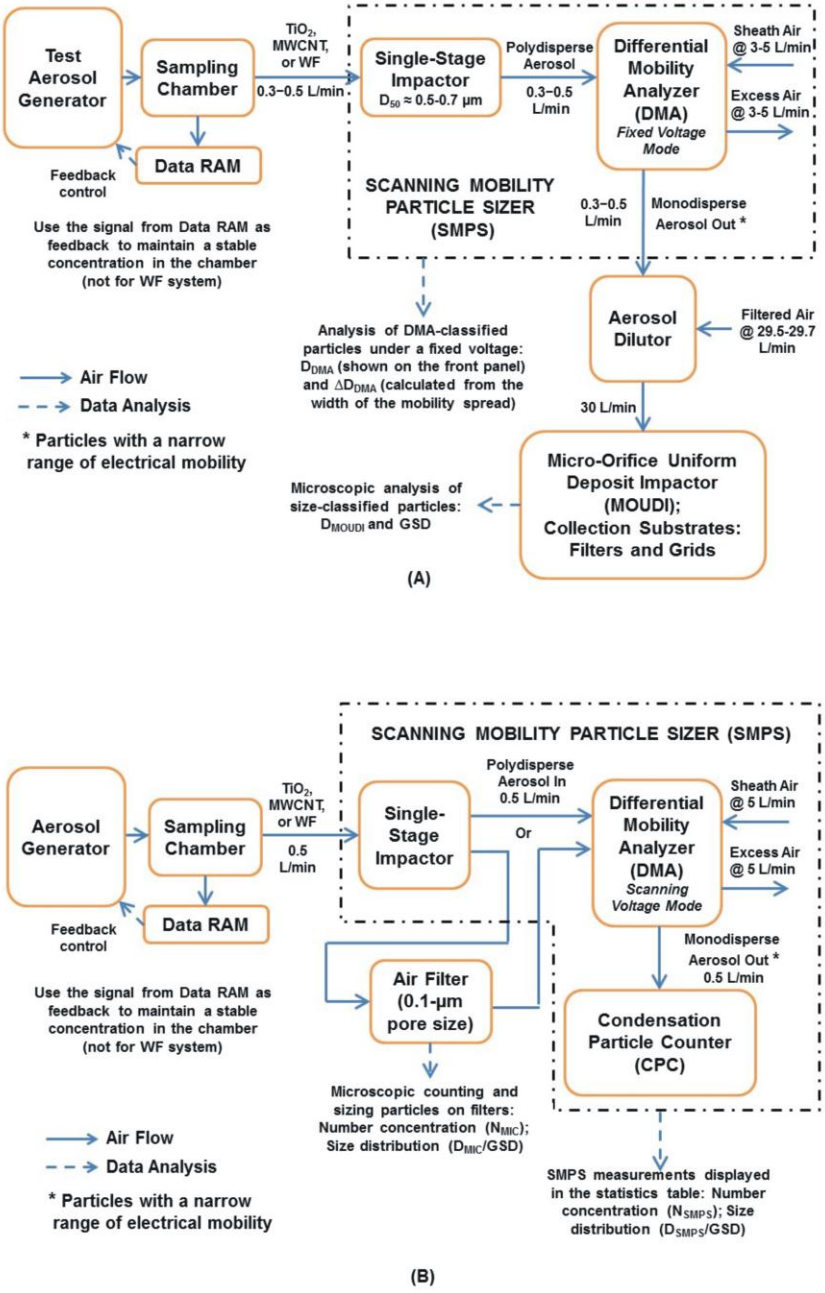

FIGURE 2. Schematic diagrams of two experimental setup for the characterization of (A) DMA-classified test aerosols [the first part of the study] and (B) overall test aerosols [the second part of the study].

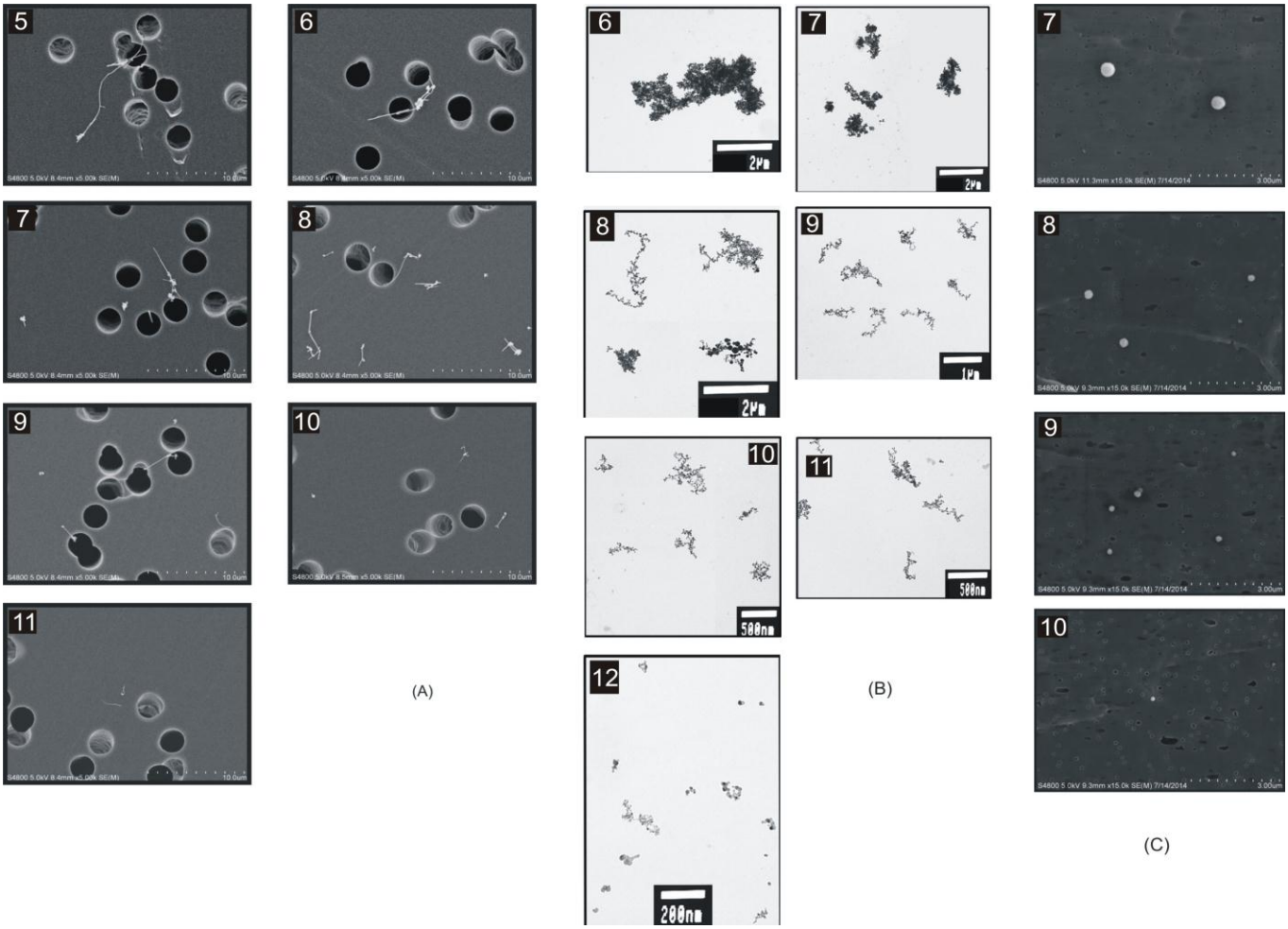

FIGURE 3. Examples of electron microscopic images of fixed-voltage DMA-classified particles distributed on various MOUDI stages: (A) at D_{DMA} = 350 nm, the MWCNT particles appear on seven stages of the impactor [5-11; 2.5-μm pore size; the full range of the tic marks = 10 μm]; (B) at D_{DMA} = 300 nm, the WF particles appear on seven stages of the impactor [6-12]; (C) at D_{DMA} = 160 nm, the TiO_2 particles appear on four stages of the impactor [7-10; 0.1-μm pore size; the full range of the tic marks = 3 μm]. Refer to the description in Table I for the stage number and the corresponding D_{50}.

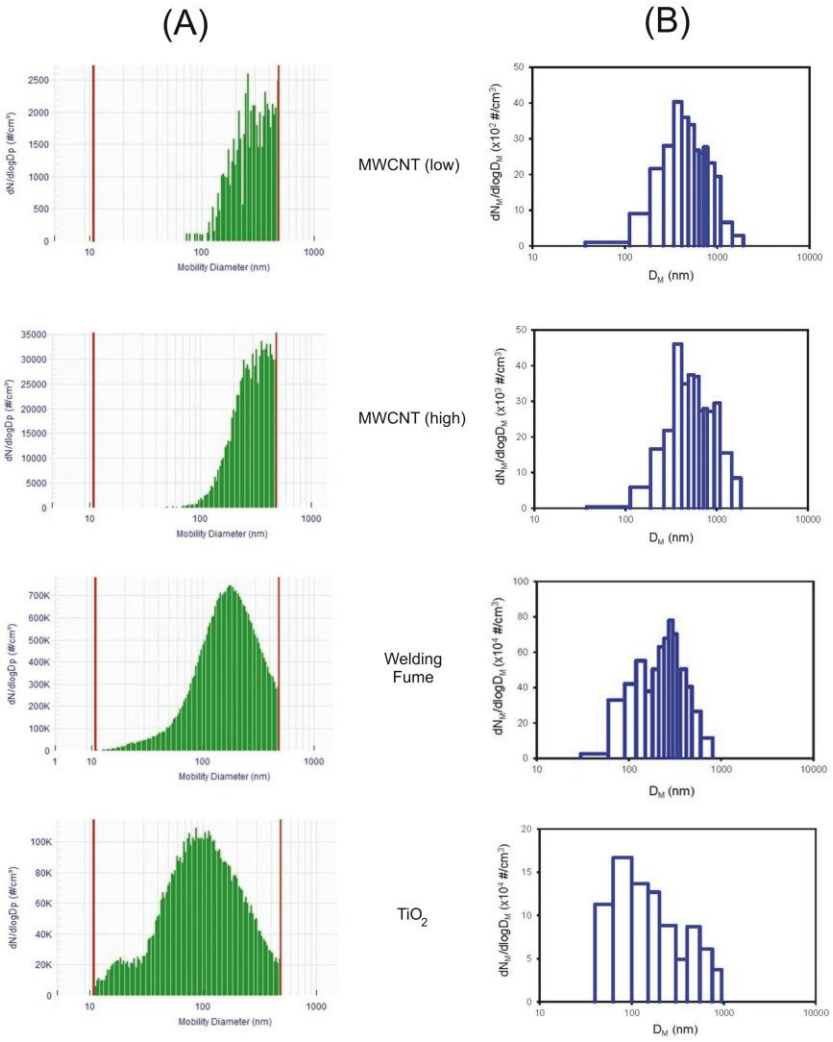

FIGURE 4. Comparison of particle size distributions between (A) SMPS graphic displays under the normal format (left) and (B) histograms based on microscopic measurements (right) for MWCNT (low), MWCNT (high), WF, and TiO_2 aerosols. N = number concentration based on SMPS, D_p = electrical mobility diameter, N_M = number concentration based on microscopic counting, D_M = diameter based on discrete particle sizing.

TABLE I. DMA-classified test aerosols (fixed voltage mode): comparison of the geometric mean diameters (D_{DMA}), calculated ranges (ΔD_{DMA}) based on electrical mobility classification[14] and the means (D_{MOUDI}), geometric standard deviations (GSD) using a MOUDI.

Aerosol	Chamber Concentration M_C (mg/m^3)	Diameter at Scanning Peak[A] (nm)	DMA Classification		MOUDI Classification		
			D_{DMA} (nm)	ΔD_{DMA} (nm)[B]	Stage[C]	D_{MOUDI} (nm)	GSD
MWCNT	6.5	350 - 354	180	175 - 186	7-11	285	1.57
			350	337 - 363	5-11[D]	301	1.78
			450	433 - 467	5-10	314	1.77
WF	4.5	180 - 182	100	97 - 103	8-12	83	1.48
			180	175 - 186	6-12	150	1.45
			300	290 - 311	6-12[D]	182	1.56
TiO_2	4.8	90 - 91	50	49 - 52	-[E]	-[E]	-[E]
			90	88 - 93	8-11	188	1.31
			160	155 - 165	7-10[D]	247	1.32

[A] The size range of the peak number concentration from the SMPS using the full scan mode. Multiple runs were conducted to ensure a steady concentration around the peak during the experiments.

[B] ΔD_{DMA} is the calculated range of mean diameter D_{DMA} expected to be extracted from the DMA at a fixed voltage setting.[14,15] A brief derivation can be found in Appendix C.[C] MOUDI stages where particles were found (Figure 3) using electron microscopes. The 50% cutoff diameters (D_{50}) for the 5th to 12th stages in MOUDI are 1.8, 1.0, 0.56, 0.32, 0.18, 0.10, 0.056, and 0.032 μm, respectively.

[D] These three samples were selected for showing particle images in Figure 3.

[E] No particles could be found on any of the MOUDI filter samples using electron microscopes.

TABLE II. Size and morphological information of test nanoparticles used in the study. Aerosols were collected on filters at the downstream of the single-stage impactor in SMPS and then examined by FE-SEM.

TiO_2	**WF**	**MWCNT (low concentration)**	**MWCNT (high concentration)**
M_C = 5.2 mg/m^3	M_C = 4.1 mg/m^3	M_C = 0.5 mg/m^3	M_C = 7.4 mg/m^3
Spherical particles: Singlets = 95.7% Doublets = 3.7% Triplets = 0.4% Quadruplets = 0.2%	Chain or cluster aggregates with primary spheres: Single sphere = 3% <10 spheres = 8%	Agglomerates with primary fibrous nanotubes: Fibrous particles[B] = 86% Single fiber = 9.2%	Agglomerates with primary fibrous nanotubes: Fibrous particles[A] = 79% Single fiber = 7.6%
The diameter with most number (mode): 89 nm	Distribution of number of spheres per particle: Mean = 240 Geometric mean = 90 Mode = 55	Aspect ratio: Geometric mean = 11	Aspect ratio: Geometric mean = 9
The smallest particle observed: 44 nm		# fibers per particle: Range: 1 - 40 Geometric mean = 5.7	# fibers per particle: Range: 1 - 45 Geometric mean = 6.3
The largest particle observed: 895 nm	Size distribution of spheres in a particle: Range: 10-80 nm Mode: 26 nm	The smallest particle observed: W = 34 nm, L = 288 nm; 1 fiber	The smallest particle observed: W = 34 nm, L = 288 nm; 1 fiber
	The smallest particle (singlet) observed: 49 nm	The largest particle observed: W = 0.8 μm, L = 12 μm; 20 fibers	The largest particle observed: W = 1 μm, L = 14.5 μm; 25 fibers
	The largest particles observed: W = 1.3 μm, L = 5.1 μm; D_M ≈ 0.8 μm		

[A] M_C = mass concentration in the sampling chamber.

[B] Aspect ratio (L/W) ≥3, where L = length and W = width.

TABLE III. Characterization of test aerosols in SMPS (scanning voltage mode) by comparing total number concentration and particle size distribution from the SMPS display to those of particles collected on filters at the downstream of the single-stage impactor and then analyzed via FE-SEM using discrete particle sizing and counting.

Aerosol	M_C (mg/m^3)	Scanning Voltage Mode			Microscopic Measurement		
		N_{SMPS} (#/cm^3)[A]	D_{SMPS} (nm)[B]	GSD	N_{MIC} (#/cm^3)[A]	D_{MIC} (nm)[B]	GSD
MWCNT	0.5	1.00 x 10^3 [5.69 x 10^2][C]	276 ± 25 [330 ± 25]	1.47 [1.37]	2.51 x 10^3	421 ± 22	1.87
	7.4	1.33 x 10^4 [8.32 x 10^3][C]	282 ± 7 [346 ± 7]	1.43 [1.32]	2.76 x 10^4	492 ± 25	1.85
WF	4.1	5.09 x 10^5 [3.74 x 10^5][C]	171 ± 1 [179 ± 1]	1.87 [2.02]	5.17 x 10^5	196 ± 10	1.88
TiO_2	5.2	1.01 x 10^5 [8.04 x 10^4][C]	96 ± 2 [101 ± 2]	2.21 [2.31]	1.40 x 10^5	115 ± 8	2.30

[A] N_{SMPS} and N_{MIC} are total number concentration values from the SMPS printouts and the microscopic measurements, respectively. Results from t-tests showed that N_{SMPS} and N_{MIC} were different for low-and high-concentration MWCNTs (p=0.002 and 0.001 respectively), and TiO_2 (p=0.004), but no significant difference was evident for WF.

[B] D_{SMPS} and D_{MIC} are geometric mean values of the particle size distributions from the SMPS printouts and the microscopic measurements, respectively. The ± values are calculated 95% confidence levels for the geometric mean.[(18)]

[C] Values in brackets represent the SMPS readings corrected using the multiple charge analysis